ACS APPLIED NANO MATERIALS

www.acsanm.org Article

Soot-Based Reduced Graphene Quantum Dot/Hemin Conjugate for Favipiravir Sensing

Indranee Hazarika,[§] Tapash Kalita,[§] Poonam Deka, Sonit Kumar Gogoi, Khaled Althubeiti, Ranjit Thakuria,* and Bedanta Gogoi*

Cite This: https://doi.org/10.1021/acsanm.1c03235 Read Online

ACCESS | Metrics & More | Article Recommendations | Supporting Information

ABSTRACT: A conjugated system was synthesized from reduced graphene quantum dot (rGQD) and hemin for the selective detection of favipiravir (Fav), an antiviral drug that has come into much attention during the year 2020 for its use as a drug against severe acute respiratory syndrome coronavirus 2 (SARS-CoV-2). The required rGQD was prepared from soot particles using Hummers' method followed by the amino-hydrothermal process. At the first step, its fluorescence was quenched by preparing the conjugate with hemin. Interestingly, the fluorescence intensity gradually increases (turn-on) with increasing concentration of Fav, and develops 9-fold higher fluorescence at 15.6 nM of Fav. The fluorescence enhancement is selective, and the limit of detection (LOD) was calculated to be about 1.96 nM. The fluorescence turn-on is governed by aggregation-induced emission (AIE), which originates from electrostatic interactions between the sensor−analyte systems. A similar fluorescence turn-on was observed for Fav in human blood plasma (BP) as well as in artificial urine (AU), which indicates that the sensor is viable in real-sample analysis. In addition to Fav, its 1:1 cocrystals with theophylline (Theo) and ferulic acid (FRA) also enhance the fluorescence in real samples with an LOD of 3.47 and 12.2 nM, respectively. Therefore, the cocrystals remain intact in biological medium and the sensor interacts with cocrystals too. The detection of Fav and its cocrystals, and the development of cocrystals as alternatives in the pharmaceutical industry, is essential considering the current COVID-19 pandemic worldwide. Therefore, the findings of this work will certainly help in developing fluorescence sensors for quantitative determination of active pharmaceutical ingredients (APIs) in real samples.

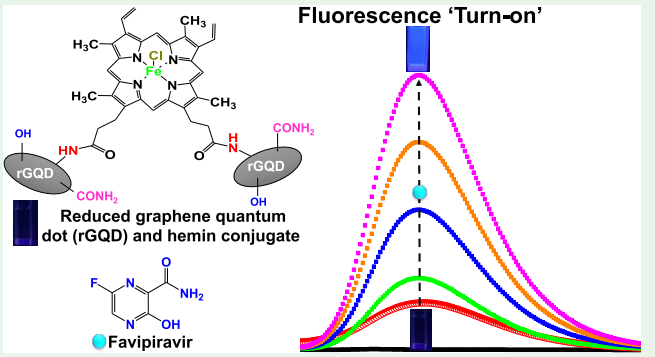

KEYWORDS: *favipiravir, cocrystal, graphene quantum dot, hydrothermal process, fluorescence turn-on, aggregation-induced emission*

INTRODUCTION

6-Fluoro-3-hydroxypyrazine-2-carboxamide, commonly known as favipiravir (Fav), is a new broad-spectrum antiviral drug manufactured by Toyama Chemicals in Japan during 2014 as an anti-influenza agent. According to the reports, it inhibits a total of 53 different types of influenza viruses[1] and was used as one of the potential drugs for the treatment of patients during the 2014 Ebola virus outbreak.[2] In addition, Fav has also been widely used in cell culture and mouse models of arenavirus, bunyavirus, filovirus, etc.[3] In recent years, Fav came into much attention due to its use in treating patients suffering from severe acute respiratory syndrome coronavirus 2 (SARS-CoV-2). According to the report by Vaidyanathan, more rigorous studies are necessary to understand the effectiveness of Fav or similar repurposed drugs for treating COVID-19.[4] There are also some reported side effects of using Fav as a drug. For example, teratogenicity and hyperuricemia are two major side effects as reported earlier.[5] Fav can cause abnormalities in the hematological parameters of COVID-19 patients. The hematological parameters include leukocyte series, erythrocyte series, platelets, and the entire blood clotting mechanisms.[6] Considering the extensive use of this drug in various diseases and also the potential side effects, it is important to develop materials and methods for its selective detection in real samples. Therefore, in this work, the prime focus is to design materials that can selectively detect Fav and/or its pharmaceutical cocrystals with theophylline (Fav•Theo) and ferulic acid (Fav•FRA) not only in aqueous solution but also in real samples. To achieve this goal, we have synthesized a conjugated system from reduced graphene quantum dots (rGQDs) and hemin.

Literature survey reveals that graphene oxide (GO), graphene quantum dots (GQDs), and rGQDs have been

Received: October 5, 2021
Accepted: November 18, 2021

Scheme 1. Pictorial Representation of the Sensing of Favipiravir and Its Cocrystals from rGQD-Hemin Conjugate via Fluorescence Turn-On Process

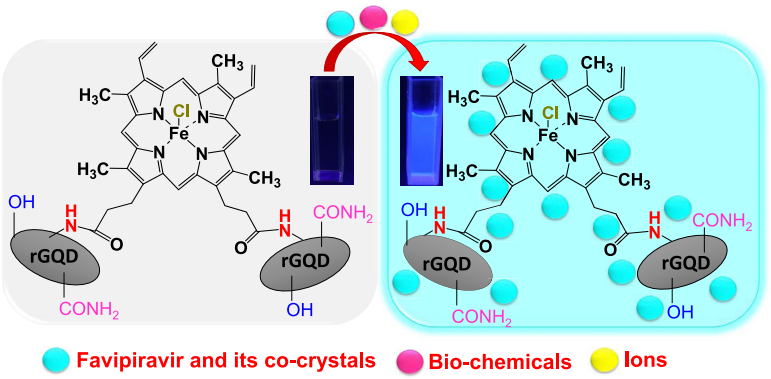

extensively used in recent times for designing various biosensors and drug detection processes worldwide. Recently, Maheshwaran et al. developed a GO-warped tetragonal t-lanthanum nanocomposite for sensing antifungal and anti-protozoal drugs.[7] Qian et al. developed a GO-based electrochemical sensor for the active pharmaceutical ingredient (API) naproxen.[8] Chihava et al. synthesized a GQD composite with nickel−cobalt sulfide for electrochemical determination of antiretroviral drugs.[9] Bharathi et al. used GQDs for ratiometric determination of the HE4 ovarian cancer biomarker.[10] Zhang et al. worked on GQD-based nanocomposites to diagnose the cancer biomarker APE1 in living cells.[11] In the past, there have been reports dedicated to the detection of various antiviral drugs such as acyclovir,[12,13] heptodin,[14] oseltamivir,[15] oseltamivir phosphate, and carboxylate,[16] etc. However, no such reports are available for the detection of Fav or any pharmaceutical cocrystal in real samples till date. As the regulatory opinion regarding pharmaceutical cocrystals has changed in the eyes of the Food and Drug Administration (FDA) and they are considered as a drug product intermediate, along with API, detection of pharmaceutical cocrystals in real samples is also necessary for solid-state drug development.[17] Furthermore, to the best of our knowledge, preparation of rGQDs from soot particles via the amino-hydrothermal process and its conjugate with porphyrins as a chemosensor has not been reported earlier. Production of soot particles is cheap and easy, and they can be a good alternative to commercially available graphite. Soot particles primarily comprise amorphous graphitic carbon with organic and inorganic materials. Therefore, they can be subjected to Hummers' method to prepare GO.[18] Post processing of GO can lead to various other materials based on the desired applications. Also, there are some advantages of using carbon-based quantum dots, such as their outstanding accessibility, stability, and biocompatibility. Preparation of GQDs is cost effective; their toxicity is low, and they possess a large specific surface area and outstanding photoelectric properties compared to the conventional quantum dots.[19]

It is well known that fluorescence turn-on-based sensing is superior to that of fluorescence turn-off-based sensing, which is attributed to a higher degree of selectivity, resolution, and lower potential errors for the former.[20] Also, fluorescence measurement-based sensing is straightforward and cost effective compared to other techniques such as high-performance liquid chromatography,[21] flow injection chemiluminescence,[22] radioimmunoassay,[23] micellar electrokinetic chromatography,[24] high-performance capillary electrophoresis,[25] etc. Therefore, the main goal of this work is to achieve fluorescence-based sensing of API and its pharmaceutical cocrystals using a fluorescence turn-on mechanism. One of the main reasons for fluorescence turn-on is aggregation-induced emission (AIE), where intramolecular rotation of the individual substances is restricted due to aggregation, which increases the photoluminescence (PL) intensity by deactivating the nonradiative emission.[26] AIE was first observed by Tang et al. in silole molecules in the year 2001,[27] and since then research efforts have been made to provide theoretical and experimental explanations for AIE. Different factors, such as structural rigidity, viscosity, temperature, and presence of chromophores in rigid matrices, can influence the aggregation and hence the fluorescence emission.[28] Due to its superior performance, many AIE molecular probes and nanomaterials have been developed for sensing, imaging, and theranostic applications.[29]

rGQDs exhibit excellent fluorescence properties, and hence different biosensors and chemosensors have already been developed earlier.[30,31] We found that, in the case of its conjugation with hemin, the fluorescence intensity of rGQDs is quenched. But, on introduction to Fav or its cocrystals, the sensor−analyte system remarkably enhances the fluorescence emission. Therefore, it would be interesting to investigate the efficacy and mechanistic details of the fluorescence turn-on process. A pictorial representation of the strategy applied for the selective detection of Fav and its cocrystals is given in Scheme 1.

EXPERIMENTAL SECTION

Material Development. All of the materials required for the synthesis were commercially available: Hemin (Himedia), human blood plasma (BP) (Sigma), ammonia 25% (Merck), H_2O_2 (Fischer Scientific), $KMnO_4$ (Rankem), H_2SO_4 (Merck), Theo (Sisco Research Laboratory, India), and FRA (Alfa Aesar). Fav is a gift from Cipla Pharmaceutical Division, Mumbai, India. All of the chemicals were used as received and without further purification.

Preparation of Reduced Graphene Quantum Dots (rGQDs). Soot particles were used as the starting material for the preparation of rGQDs. The required soot particles were collected from a kerosene oil lamp and stored in a desiccator over calcium chloride ($CaCl_2$). In the first stage, graphene oxide (GO) and graphene quantum dots (GQDs) were synthesized from soot particles via the well-known Hummers' method.[32] Soot particles of weight 0.10 g were mixed with 15 mL of ice-cold H_2SO_4 (98%) and stirred for 1 h (speed: 280 rpm), followed by slow addition of 0.3 g of crystalline $KMnO_4$. The material was stirred again for another 3 h. To this solution, 25 mL of deionized

https://doi.org/10.1021/acsanm.1c03235
ACS Appl. Nano Mater. XXXX, XXX, XXX−XXX

Scheme 2. Schematic Representation of (a) Synthesis of GO and GQDs from Soot Particles by Hummers' Method Followed by Amino-Hydrothermal/Hydrothermal Cutting to Produce rGO and rGQDs and (b) Synthesis of rGQD-Hm Conjugate Via Acetylation Reaction

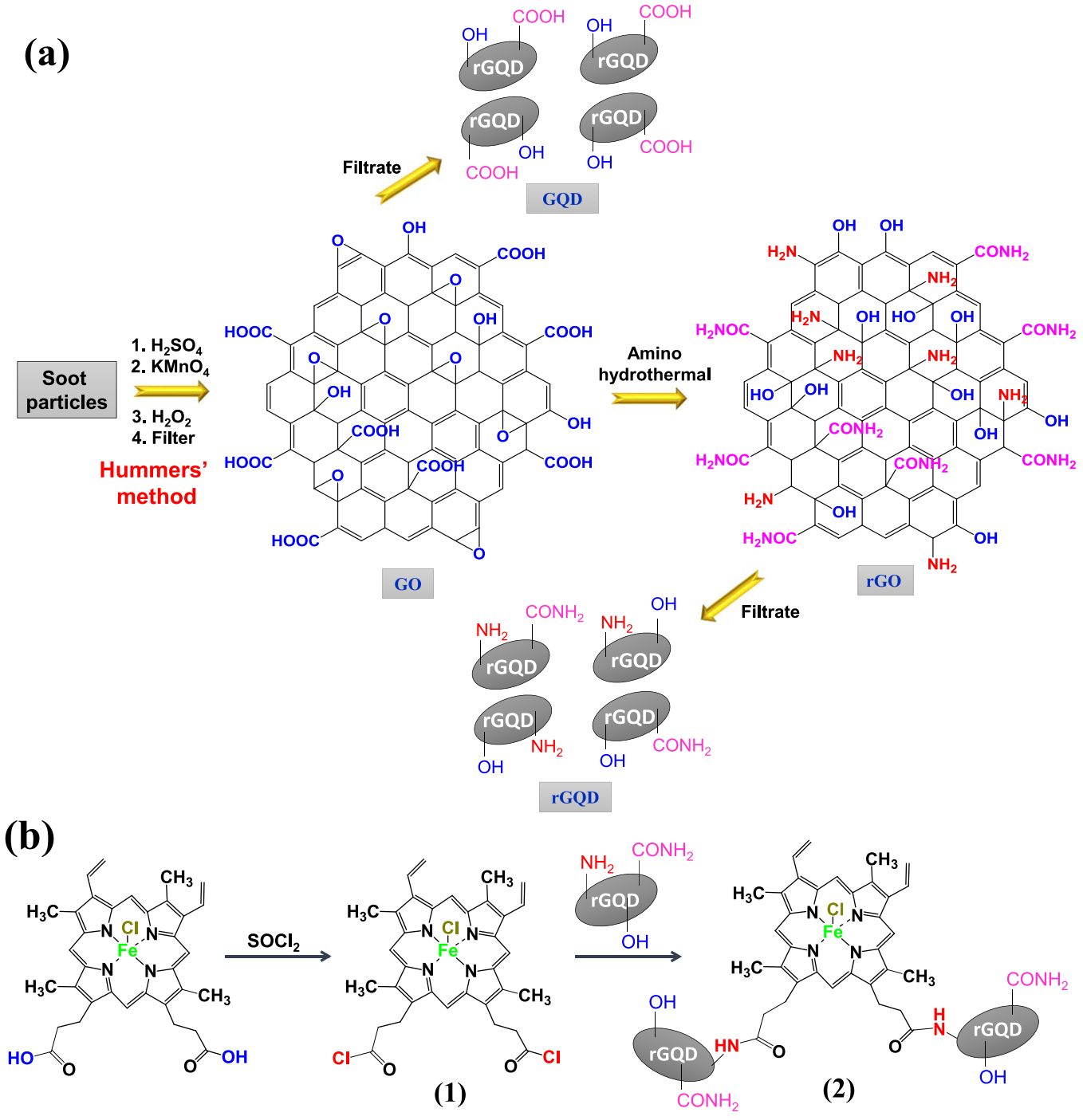

water was added slowly and heated up to 40 °C. The solution was further diluted with 25 mL of deionized water. To remove the excess $KMnO_4$, 3 mL of 30% H_2O_2 was added to the solution and filtered through a Whatman no. 42 filter paper. The residue that contained GO was washed with distilled water several times to remove the excess ions, dried in an oven at 60 °C, and stored in a desiccator over $CaCl_2$.

In the second stage, rGQDs were prepared using a high-temperature amino-hydrothermal process[33] as shown in Scheme 2a. Briefly, GO solution was prepared by dispersing 10 mg of GO in 10 mL of distilled water followed by sonication. 10 mL of distilled water and 8 mL of ammonia solution were added to it and stirred further for 30 min. The solution was then sonicated for another 30 min, transferred to a Teflon-lined autoclave, and digested at 150 °C for 5 h by hydrothermal treatment. The autoclave digester was allowed to cool to room temperature and finally, the resultant solution was filtered through the Whatman no. 42 filter paper. The filtrate was centrifuged at 8000 rpm to remove the larger particles and then used in the later stage to synthesize the conjugate with hemin.

Preparation of rGQD-Hemin (rGQD-Hm) Conjugate (2). The rGQD-Hm conjugate was essentially synthesized by performing an acetylation reaction of hemin in the first step. The simple protocol of the reaction involves the conversion of the −COOH groups of hemin to −COCl groups as shown in Scheme 2b. Here, 0.1 g of hemin was

https://doi.org/10.1021/acsanm.1c03235
ACS Appl. Nano Mater. XXXX, XXX, XXX−XXX

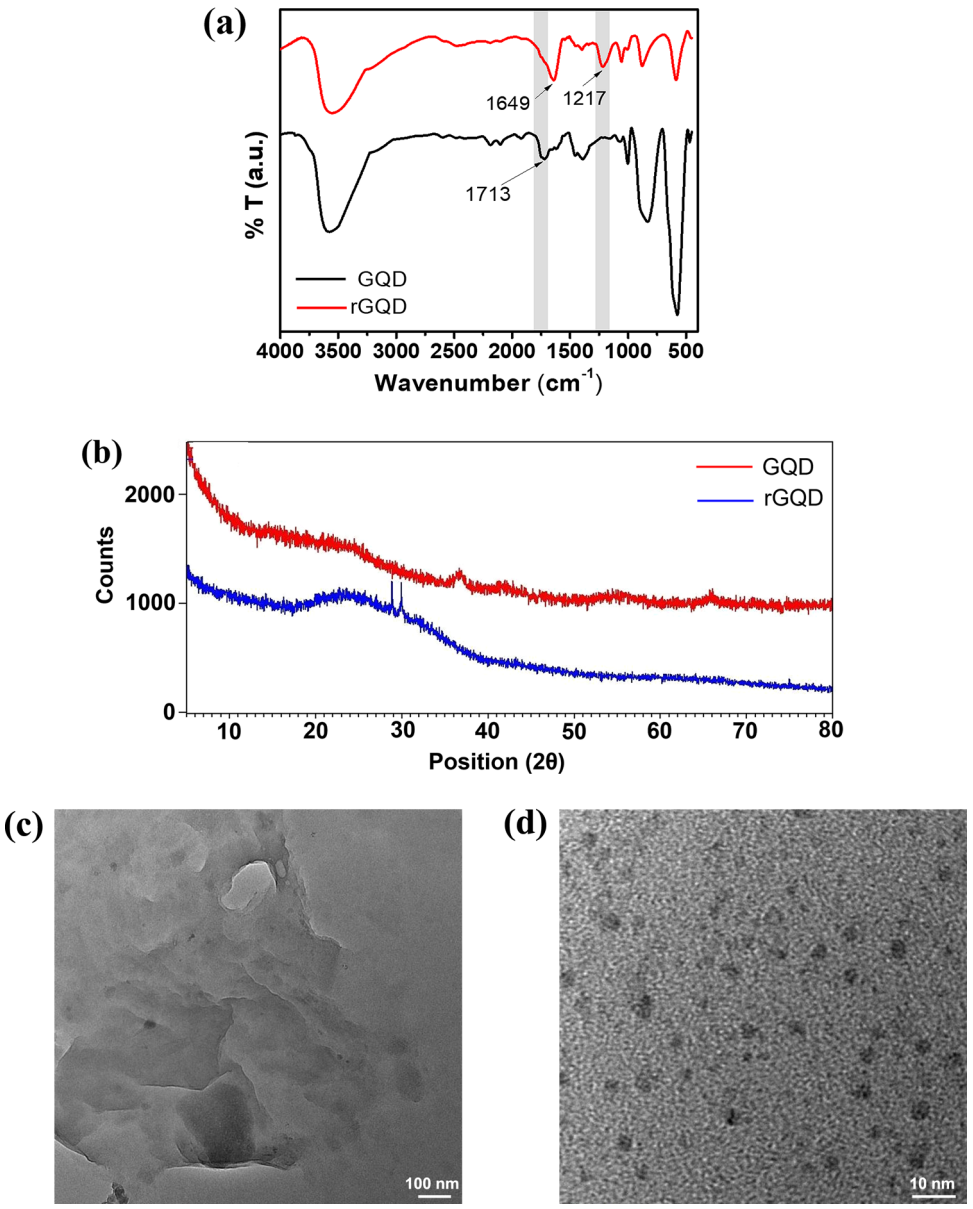

Figure 1. (a) FT-IR spectra of GQDs and rGQDs; (b) PXRD pattern of GQDs and rGQDs. TEM image of (c) GO prepared from kerosene soot using Hummers' method, and (d) rGQDs prepared using the amino-hydrothermal process.

dissolved in 10 mL of dichloromethane (DCM) at 60 °C. 2 mL of thionyl chloride ($SOCl_2$) was then added to the prepared hemin solution, and the solvent was evaporated. This produces the acid chloride derivative of hemin (i.e., hemin-COCl), designated as (1). At the final step, the rGQD-Hm conjugate was synthesized by stirring the mixture of the 10 mL rGQD solution with hemin-COCl at room temperature. As shown in Scheme 2b, the reaction between the −COCl group of (1) and the $-NH_2$ groups of the rGQD solution results in the final product. The resulting brown-colored solution was centrifuged at 8000 rpm to remove the unreacted compound (1). The remaining solution of the rGQD-Hm conjugate, designated as (2), was stored in a refrigerator for all photophysical measurements and electrical characterizations.

Material Characterization. Structural characterization of the materials was performed using the Fourier transform infrared spectroscopic technique (PerkinElmer FT-IR spectrophotometer) by preparing pellets with KBr. The measurements were performed in transmittance mode over 32 scans. Electronic transitions of the samples in aqueous media were recorded at room temperature using a UH5300 Hitachi Spectrophotometer. Steady-state fluorescence measurements were performed using a Hitachi F-7000 fluorescence spectrophotometer with 5 nm excitation and emission slit width, and at 400 V operating voltage. The fluorescence decay profiles of the samples were recorded using Fluorolog-3 (Horiba Instruments) at 700 mV operating voltage. The powder X-ray diffraction (PXRD) measurements were performed on a Rigaku Ultima IV powder X-ray diffractometer by operating a Cu Kα X-ray source equipped with an Ni filter to suppress K_β emission and a D/teX Ultra high-speed position-sensitive detector, and measurements were performed at room temperature, with a scan range 2θ = 5−80°, step size of 0.02°, and a scan rate of 10°/min. Dynamic light scattering (DLS) measurements were performed to determine the zeta potential (ξ)- and particle size of the system using Malvern NanoZS90. The samples present in aqueous media were put in a quartz cuvette having a square aperture with a zeta dip cell electrode at room temperature. The average size of the rGQDs was determined from the transmission electron microscope (TEM) images collected using JEOL TEM-2100 model. The aqueous sample was drop-casted on a 3 mm copper grid covered with a carbon film and dried under the infrared lamp.

https://doi.org/10.1021/acsanm.1c03235
ACS Appl. Nano Mater. XXXX, XXX, XXX−XXX

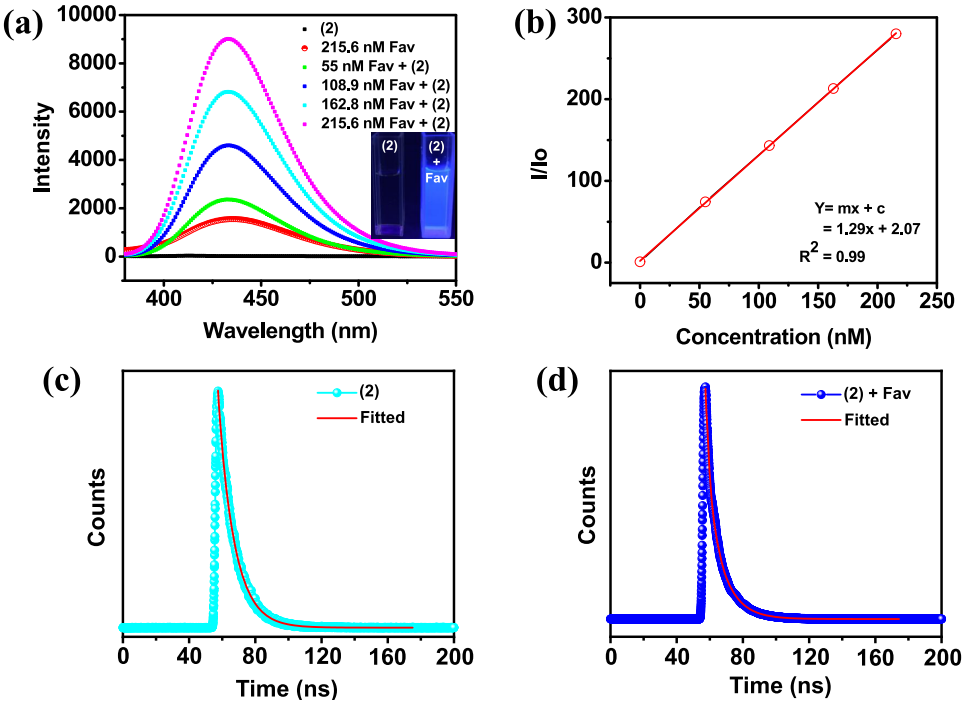

Figure 2. (a) Fluorescence spectra of conjugate (2) with increasing concentration of Fav (λ_{ex} = 360 nm) at pH 7. The red-colored curve represents the emission spectra of Fav alone in aqueous media. (b) Calibration plot obtained from the emission spectra at different concentrations of Fav to determine the limit of detection. Fluorescence decay profiles of (c) conjugate (2), and (d) conjugate (2) + 55 nM of Fav.

Sensing Experiments. *Fluorescence Sensing.* A stock solution of Fav with 0.1 mM concentration was prepared in water and used for all of the sensing experiments. 2 mL of the conjugate (2) was poured in a quartz cuvette with (4 × 1 × 1) cm area, and its emission spectra were recorded at 360 nm excitation wavelength (λ_{ex}). To it, Fav was gradually added by maintaining the concentrations at 55, 108.9, 162.8, and 215.6 nM. The emission spectra of phase-pure Fav were recorded at 215.6 nM concentration without the presence of the conjugate (2). The same protocol was followed for the sensing study of the respective cocrystals of Fav (Fav•Theo and Fav•FRA). For the real-sample analysis, the fluorescence sensing experiments were carried out in a 1:3 (V/V) mixture of the sample with blood plasma (BP) and artificial urine (AU).

RESULTS AND DISCUSSION

Material Characterization. As described earlier, GO and GQDs were synthesized from soot particles by subjecting them to the well-known Hummers' method, followed by amino-hydrothermal reaction of GO to produce rGQDs. Though GO and GQDs were not the materials of interest in this work, their characterization is essential for the structural confirmation of rGQDs and to determine the change in the surface functionalities after their formation. Here, the synthesized GQDs and rGQDs were characterized using various spectroscopic techniques, such as UV−visible, FT-IR, PL spectroscopy, and PXRD. The UV−vis spectra of GQDs and rGQDs possess sharp peaks at ca. 226 and 229 nm, respectively, as shown in Figure S1a,b. These peaks correspond to the $\pi-\pi^*$ transition, the characteristics of GQDs and their reduced form.[34] The optical band gaps calculated based on the UV−vis spectra of the respective GQDs and rGQDs using Tauc plot[35] were found to be 4.67 and 4.88 eV. Both GQDs and rGQDs show excitation wavelength (λ_{ex})-dependent emission spectra as shown in Figure S1c,d. It is evident that, with increasing λ_{ex}, the position of the emission spectra undergoes a red shift along with a gradual decrease in spectral intensity. This indicates that there is a strong dependence of fluorescence on the excitation wavelength. This process is commonly known as the "giant red-edge effect", exhibited by materials such as GO, GQDs, and carbon dots.[36]

Structural characterization of GQDs and rGQDs was carried out using FT-IR spectra as shown in Figure 1a. Due to the presence of a broad peak at ∼3500 cm^{-1} corresponding to O−H stretching, it is difficult to identify the N−H functional in the rGQDs. The appearance of a new peak at 1217 cm^{-1} w.r.t. the FT-IR spectrum of the GQDs confirms the presence of an aromatic amine[37] in the rGQDs. Moreover, the shift in the C═O stretching peak from 1713 cm^{-1} (corresponding to the COOH group)[38] of GQDs to 1649 cm^{-1} (corresponding to the $CONH_2$ group)[39] confirms the formation of rGQDs. Reduction of GQDs could also be confirmed from the relative intensities of the peaks corresponding to the C−O frequencies of the epoxide linkages at 1004 cm^{-1} for GQDs and 1054 cm^{-1} for rGQDs.[37] PXRD analysis (Figure 1b) showed a broad hump at ∼20−35° 2θ, corresponding to the amorphous nature of the synthesized rGQDs.

Apart from the change in surface functional groups, the most important criterion for the formation of rGQDs is a reduction in the size of GO after the amino-hydrothermal reaction, which is characterized using TEM. The 2D-sheet-like structure of GO (Figure 1c) obtained from kerosene soot particles using Hummers' method showed a characteristic change, with a reduction in particle size to nearly about 5 nm average corresponding to rGQDs. Moreover, Figure 1d shows a uniform distribution of the spherical-shaped particles of rGQDs compared to GO. The high-resolution TEM (HRTEM) image of the rGQDs is presented in Figure S2. Photophysical and structural characterization of the conjugate (2) was carried out using UV−vis, PL, and FT-IR analysis as described in the following section.

https://doi.org/10.1021/acsanm.1c03235
ACS Appl. Nano Mater. XXXX, XXX, XXX−XXX

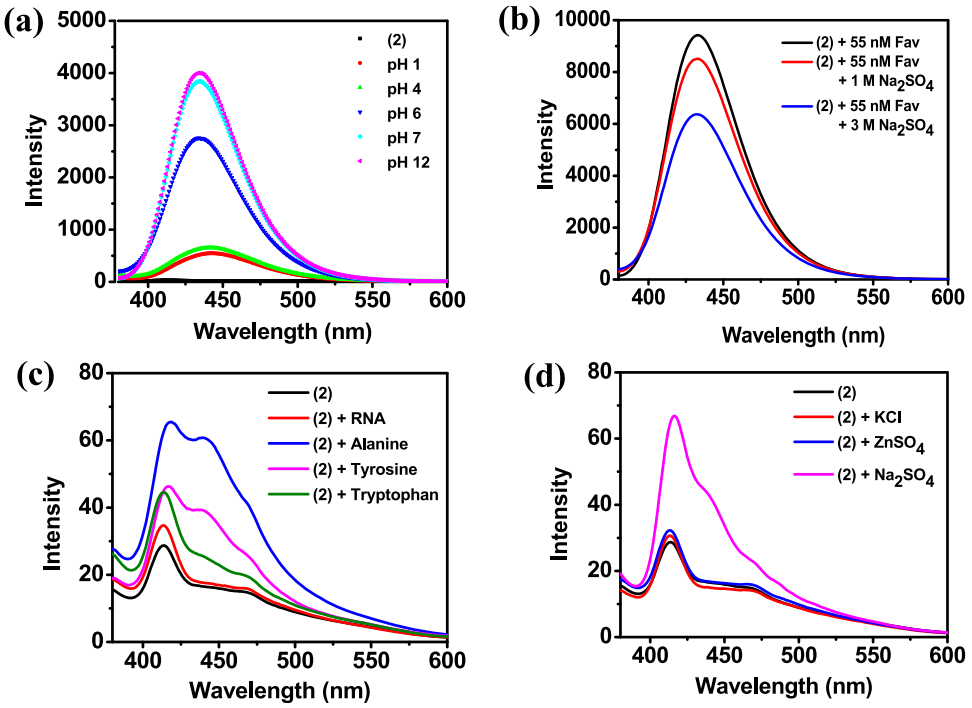

Figure 3. Comparison of the (a) emission spectra of conjugate (2) with Fav (108.9 nM) at different pH; (b) fluorescence spectra of conjugate (2) at 55 nM of Fav with increasing concentration of Na_2SO_4; fluorescence spectra of conjugate (2) (c) in the presence of RNA, alanine, tyrosine, and tryptophan in aqueous media, and (d) in the presence of 0.1 mM of KCl, $ZnSO_4$, and Na_2SO_4.

From the UV−vis spectral analysis, we found that the conjugate possesses a strong absorption in the range of 200−300 nm, and the corresponding optical band gap calculated from the Tauc plot was found to be ∼2.9 eV (Figure S3a). On the other hand, the conjugate (2) possesses interesting fluorescence property. As shown in Figure S3b, the intensity of the emission spectra of the conjugate is very poor compared to the rGQDs in aqueous media, and undergoes a red shift with increasing excitation wavelength from 300 to 360 nm, which is the characteristic property of rGQDs. The formation of the acid chloride of hemin (1) and the conjugate (2) has been confirmed with the help of their respective FT-IR spectra. Crystalline hemin possesses a distinct peak at 1700 cm^{-1} corresponding to carboxylic acid C═O stretching (Figure S3c). After the reaction of the −COOH groups with $SOCl_2$, the shifting of the peak to 1732 cm^{-1} in compound (1) confirms the formation of the acid chloride functional. The shifting of the peak again to 1713 cm^{-1} in (2) might be due to the presence of unreacted COOH groups. Another characteristic peak of (1) at ∼800 cm^{-1} corresponding to the C−Cl stretching vibration confirms the presence of the acid chloride functional, which is absent in conjugate (2). Moreover, conjugate (2) contains three new peaks at 1657, 1560, and 660 cm^{-1} corresponding to the C═O stretching of the amide groups, NH bending of the secondary amide, and NH out-of-plan bending, which are absent in the FT-IR spectrum of compound (1).[37]

Sensing Studies Via Fluorescence Measurements. Fluorescence turn-on sensing is generally achieved via quenching the fluorescence of rGQDs at the first step followed by addition of the analyte. It was observed that with the gradual increase in the concentration of the analyte, Fav, the emission of conjugate (2) drastically increases, and at a maximum concentration of 215.6 nM, the system attains a 9-fold enhancement in fluorescence intensity compared to the fluorescence of Fav alone with the same concentration. Therefore, the system essentially follows a fluorescence "turn-on" pathway in the sensing process. rGQDs alone also show fluorescence turn-on in the presence of Fav (see Figure S4), but the extent of fluorescence enhancement is not as efficient as that of the conjugate. This is presumably due to the extensive interaction between the analyte and conjugate (2) with a larger chemical structure. The addition of Fav into conjugate (2) leads to a bright fluorescence under UV light at 265 nm monochromatic light as shown in the inset of Figure 2a. From the calibration curve for varying concentrations of Fav, the limit of detection (LOD) was calculated using the formula LOD = 3.3 σ/S, where S is the slope of the plot and σ is the relative standard deviation (RSD). In this system, the LOD was calculated to be about 1.96 nM using a calibration plot.[40] For all concentrations of Fav, the fluorescence turn-on is instantaneous and no further increase in the intensity was observed. The increase in fluorescence intensity of conjugate (2) with increasing concentration of Fav follows a linear trend with a regression coefficient of 0.99, as is evident from the calibration curve (Figure 2b).

Considering the possible chemical structure of the conjugate with a hemin moiety and the rGQDs, the fluorescence turn-on in the presence of Fav is presumably due to aggregation of the sensor−analyte system as discussed in the Introduction. As a proof of concept, we have determined the fluorescence lifetime of the system and performed DLS measurements before and after the sensing experiments. From the fluorescence decay profiles (Figure 2c,d), the initial fluorescence lifetime of the conjugate was calculated to be 5.8 ns, which increases to 6.04 ns after the interaction with the conjugate. Such increase in the fluorescence lifetime is observed in aggregated systems where the nonradiative pathways are blocked due to the aggregation

https://doi.org/10.1021/acsanm.1c03235
ACS Appl. Nano Mater. XXXX, XXX, XXX−XXX

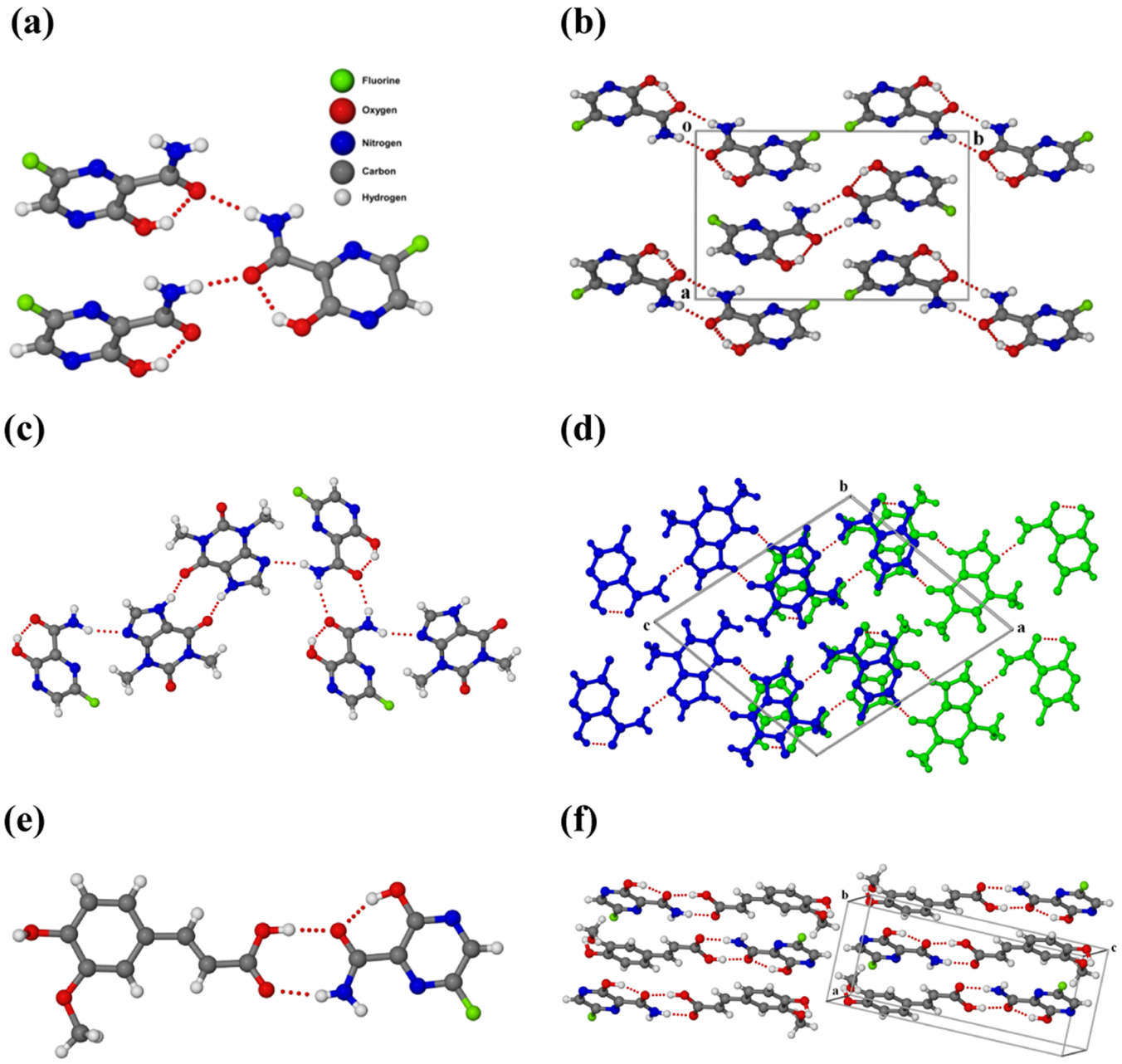

Figure 4. Hydrogen bond interactions and molecular packing of (a, b) Fav and the respective cocrystals; (c, d) Fav•Theo; and (e-f) Fav•FRA. Red, green, blue, gray, and white color balls denote oxygen, fluorine, nitrogen, carbon, and hydrogen atoms, respectively.

and hence the molecules are present in the excited state for a longer time, thereby increasing the fluorescence lifetime.[41]

Another important aspect of the sensing process is to investigate the change in particle size and zeta potential (ζ)-of the system with the help of DLS measurements to confirm the sensor−analyte aggregation. It was found that in aqueous media, the value of ζ of the conjugate (2) is about −23 mV, which decreases to −16 mV after the introduction of Fav (Figure S5a,b). Similar ζ values were obtained in repetitive measurements. This clearly reveals the occurrence of electrostatic interactions in the system similar to that in the earlier reports;[42−44] moreover, a lower negative value of ζ can lead to particle aggregation in the system.[45] This assumption is in agreement with the results of particle-size measurements. As evident from Figure S5c,d, the average particle size of the conjugate drastically increases from 160 to 777 nm after the interaction with Fav (215.6 nM). This is a significant increase in terms of particle size that causes the fluorescence turn-on of the system. Similarly, under TEM, highly aggregated particles were observed after the interaction of conjugate (2) with Fav as shown in Figure S6a,b. From these two observations, it can be concluded that AIE is the underlying mechanism involved in the enhancement of fluorescence intensity. On the other hand, the peak positions in the FT-IR spectra of the conjugate remain the same before and after the interaction with Fav, which indicates that there is no change in the functionalities of the conjugate after the sensing (Figure S7).

It was found that the pH of the solution plays a vital role in the efficiency of the fluorescence enhancement. The maximum fluorescence enhancement occurs at neutral as well as basic pH values as shown in Figure 3a. It is important to mention that hemin is soluble in aqueous media at basic pH.[46] Therefore, at

https://doi.org/10.1021/acsanm.1c03235
ACS Appl. Nano Mater. XXXX, XXX, XXX−XXX

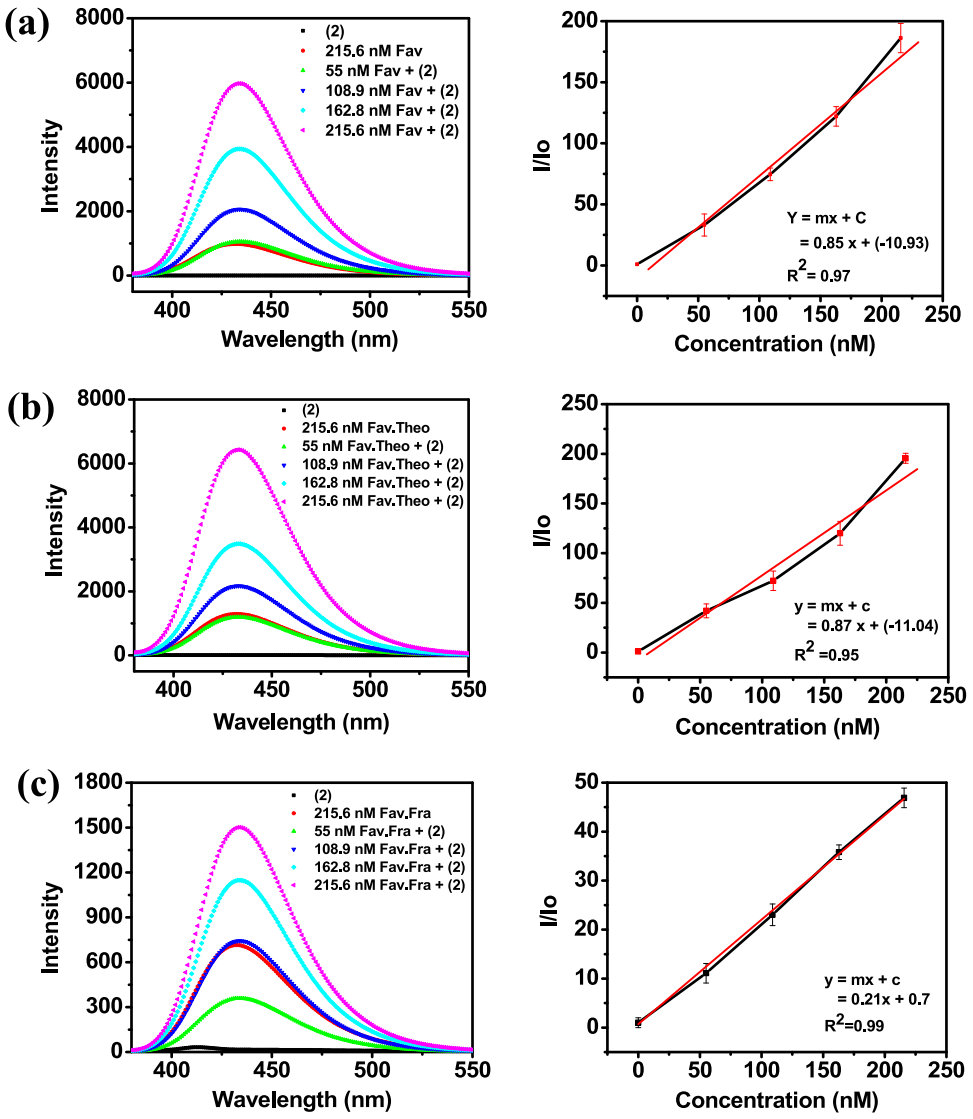

Figure 5. Real-sample analyses: fluorescence sensing and calibration curves in AU for (a) Fav, (b) Fav•Theo, and (c) Fav•FRA.

acidic pH, conjugate (2) is not fully soluble in water, which probably leads to a poor interaction with the analyte and hence no such fluorescence turn-on was observed at pH 1 and 4. The existing emission at these pH values is due to the presence of Fav itself in the solution. In neutral and basic pH range, the fluorescence enhancement is presumably due to the AIE mechanism resulting from a combined effect of the electrostatic interactions in the sensor−analyte system as well as the solution-phase fluorescence of Fav. The occurrence of electrostatic interaction was experimentally confirmed by performing the well-known "salt-screening effect" experiment. Here, the fluorescence response for Fav (55 nM) in the presence of high concentrations of a salt solution (1 and 3 M of Na_2SO_4) was observed. According to the literature, the presence of a highly concentrated salt solution hinders the electrostatic interaction between the sensor and the analyte and thereby reduces the fluorescence intensity.[42] In our case, it was observed that the initial fluorescence intensity in the presence of Fav significantly decreases with the increasing concentration of the salt solution as shown in Figure 3b.

To investigate the selectivity of the sensor for Fav, fluorescence measurements were performed for other biologically important compounds such as RNA, alanine, tyrosine, and tryptophan. As evident from Figure 3c, no significant enhancement in fluorescence intensity was observed for such chemicals. Since Fav contains an amide group in its chemical structure, we also performed sensing experiments for other amide functional drugs, namely carbamazepine (Carb), 2-ethoxybenzamide (Etha), and pyrazinamide (Pyr). It was observed that among them fluorescence turn-on was found only in the case of Fav (Figure S8). Therefore, it can be stated that the method is highly selective. On the other hand, since analytical samples might contain additional ions in low concentrations, we extended the sensing experiment in the presence of 0.1 mM concentration of KCl, $ZnSO_4$, and Na_2SO_4 too. As shown in Figure 3d, the changes in fluorescence intensities in the presence of these ions were negligible.

In the present sensor−analyte system, the presence of a fluorophore analyte is essential for the sensing process. In order to establish our claim, we performed additional sensing experiments using two cocrystals of Fav along with the respective coformers as independent analyte systems. Cocrystallization is a useful tool to tune the photophysical properties of an individual fluorophore. Using the concept of cocrystal-

https://doi.org/10.1021/acsanm.1c03235
ACS Appl. Nano Mater. XXXX, XXX, XXX−XXX

lization, Yan et al. tuned the luminescence properties of stilbene-type organic solid-state materials.[47] As Fav shows weak solution-phase fluorescence, cocrystals of Fav will definitely affect its photophysical property. In a very recent report, we investigated the physicochemical properties of a few cocrystals of Fav with generally regarded as safe (GRAS) coformers.[48] From the reported cocrystal system, we selected two Fav cocrystals, viz. 1:1 cocrystals of Fav•Theo and Fav•FRA, which showed significant changes in fluorescence intensity (Figure S9). Along with the two cocrystals, we also investigated the sensing experiment for the respective coformers (Theo and FRA). This is to establish whether the change in the photophysical property of the cocrystal is due to the presence of individual coformers or structural changes observed based on cocrystallization. The crystal packing arrangement of Fav and the respective cocrystals is shown in Figure 4 along with their possible hydrogen bond interactions.

Theo and FRA do not show any solution-phase fluorescence; hence, no characteristic fluorescence turn-on behavior has been observed for their complexes with conjugate (2) (Figure S9). On the other hand, Fav cocrystals showed the fluorescence turn-on behavior. In the presence of conjugate (2), the intensity of the fluorescence emission of the 1:1 Fav•Theo cocrystal is higher than that of the 1:1 Fav•FRA cocrystal; the same is the case for their respective fluorescence in aqueous medium. The observed result clearly supports the existence of cocrystals in the solution phase,[49] as well as the necessity of a fluorophore analyte for sensing activity.

Practical Applicability of the Sensor. After establishing the underlying mechanism and specificity of the system, we further investigated the practical applicability of the sensor for detecting Fav and its cocrystals in biological samples. In general, biological samples contain additional proteins, salts, nucleic acids, etc. along with the analyte, which may affect the sensing activity during the investigation. Therefore, it is always recommended to perform sensing measurements in real samples to investigate the practical applicability of the designed sensor. The fluorescence turn-on-based sensing process, being selective towards a particular analyte, is more promising in this regard. As mentioned earlier, to check the sensitivity in real samples, we performed sensing experiments in the presence of AU and BP. AU contains components such as urea, uric acid, creatinine, $Na_3C_6H_5O_{72}·H_2O$, NaCl, etc.;[50] on the other hand, BP is a pale yellow medium that contains many organic and inorganic components, amino acids, salts, proteins, etc.[51] Despite the presence of various components, the conjugate−analyte system shows significant enhancement in fluorescence intensity for Fav as well as its cocrystals both in AU and BP, as depicted in Figure S10a. Therefore, it can be concluded not only that the interference of other components towards the detection of Fav and its cocrystals is negligible, but also that the sensor system is effective in a real biological medium. After confirming the applicability of the sensor in AU and BP, the fluorescence enhancement in AU with increasing concentrations of Fav, Fav•Theo, and Fav•FRA was recorded to measure the LOD. Figure 5a−c shows the fluorescence sensing and calibration curve of Fav, Fav•Theo, and Fav•FRA, respectively, in AU. Here, three consecutive measurements were performed to determine the calibration curves, and the standard deviation was included as *Y*-error for every concentration of Fav. These calibration plots also follow a linear trend, and the LOD was calculated to be about 3.5, 3.47, and 12.2 nM, respectively. Here, the fluorescence enhancement in the case of the Fav•FRA cocrystal is not as efficient as those for Fav and Fav•Theo though the LOD was calculated to be in the nanomolar range. The sensing study for Fav cocrystals in AU and BP also suggested the better stability and existence of pharmaceutical cocrystals in real biological medium.

To study the stability of the conjugate, the same stock solution was used for recording the fluorescence spectra after completing 60 days of the synthesis under identical conditions and instrumental parameters. The conjugate−analyte complex showed a similar fluorescence enhancement (Figure S10b). Based on our observation, we can conclude that the conjugate was effective and stable for up to a period of 2 months.

CONCLUSIONS

In summary, a new conjugate of rGQDs with hemin is reported. Soot particles were used as the starting material for the synthesis of rGQDs with the help of Hummers' method followed by the amino-hydrothermal process. The conjugate is an efficient sensing platform for selective detection of Fav and its cocrystal in aqueous media as well as simulated biological media. The rGQD is a fluorescent material and its conjugate is prepared to achieve the non-fluorescent conjugate required for the sensing of the fluorescent Fav molecule. The sensing is based on fluorescence turn-on of the conjugate in presence of a nanomolar concentration of the analyte which is attributed to AIE that enables the sensor to be applicable in real samples such as BP and AU. The LOD of the system for Fav in aqueous media and AU was found to be 1.96 and 3.5 nM respectively. Similarly, the sensing measurements were performed for Fav•Theo and Fav•FRA cocrystals in AU and the LOD for these two analytes were found to be 3.47 and 12.2 nM respectively. The results are reproducible and selective which are the primary requisites for developing efficient sensors. Cocrystal sensing showed better stability of cocrystals in biological medium and their usefulness as a drug product intermediate. In continuation to this work, we will focus on developing electronic device based sensing platform for the detection of Fav or similar APIs in real samples. Again, since hemin is an important bio-based material, the initial fluorescence quenching of rGQDs during the preparation of the conjugate with hemin acetyl chloride indicates the possible applicability of rGQDs as a biosensor for hemin. The rGQDs also showed fluorescence turn-on in the presence of Fav to some extent. Therefore, extensive study is necessary to establish the mechanism; however, it is out of the scope of this present study. Future studies can also be directed towards the investigation of the efficiency of pharmaceutical cocrystals as repurpose drugs. From an environmental perspective, it is well-known that soot particles are carcinogenic and one of the major contributor towards global warming. Therefore, the extraction and conversion of soot particles into useful materials may lead to sustainable product development.

ASSOCIATED CONTENT

Supporting Information

The Supporting Information is available free of charge at https://pubs.acs.org/doi/10.1021/acsanm.1c03235.

Photophysical characterization of GQD and rGQD; high-resolution transmission electron microscope (HRTEM) image of rGQD; characterization of the conjugate (2); sensing experiments of rGQD with Fav;

https://doi.org/10.1021/acsanm.1c03235
ACS Appl. Nano Mater. XXXX, XXX, XXX−XXX

dynamic light scattering (DLS) measurements; transmission electron microscopic (TEM) analysis before and after sensing of Fav; FT-IR spectra of the conjugate (2) before and after sensing of Fav; selectivity test with amide containing drug molecules; fluorescence sensing experiments for crystals and coformers; fluorescence studies in real samples and stability test (PDF)

AUTHOR INFORMATION

Corresponding Authors

Ranjit Thakuria − *Department of Chemistry, Gauhati University, Guwahati 781014 Assam, India*; Email: ranjit.thakuria@gmail.com, ranjit.thakuria@gauhati.ac.in

Bedanta Gogoi − *Department of Chemistry, Gauhati University, Guwahati 781014 Assam, India*; orcid.org/0000-0002-2450-8322; Email: bedanta@gauhati.ac.in

Authors

Indranee Hazarika − *Department of Chemistry, Gauhati University, Guwahati 781014 Assam, India*

Tapash Kalita − *Department of Chemistry, Gauhati University, Guwahati 781014 Assam, India*

Poonam Deka − *Department of Chemistry, Gauhati University, Guwahati 781014 Assam, India*

Sonit Kumar Gogoi − *Department of Chemistry, Gauhati University, Guwahati 781014 Assam, India*

Khaled Althubeiti − *Department of Chemistry, College of Science, Taif University, Taif 21944, Saudi Arabia*

Complete contact information is available at: https://pubs.acs.org/10.1021/acsanm.1c03235

Author Contributions

§I.H. and T.K. contributed equally.

Notes

The authors declare no competing financial interest.

ACKNOWLEDGMENTS

I.H. (Ph.D. scholar) acknowledges the DST, Government of India, for providing fellowship. B.G. acknowledges the DST, Government of India, for providing financial support under the INSPIRE faculty scheme (IFA18-CH 313). B.G. and R.T. are also grateful to the Department of Chemistry, Gauhati University, for providing laboratory facilities and powder X-ray diffractometer; Sophisticated Analytical Instrumentation Facility (SAIF), Gauhati University, for the single crystal X-ray diffractometer. K.A. thanks Taif University Researchers Supporting Project Number TURSP-2020/241, Taif University, Taif, Saudi Arabia. P.D. thanks the UGC for the Junior Research Fellowship (Ph.D. scholar). The Institute of Advanced Study in Science and Technology (IASST) is acknowledged for collecting the TEM images.

REFERENCES

(1) Sleeman, K.; Mishin, V. P.; Deyde, V. M.; Furuta, Y.; Klimov, A. I.; Gubareva, L. V. In vitro antiviral activity of favipiravir (T-705) against drug-resistant influenza and 2009 A (H1N1) viruses. *Antimicrob. Agents Chemother.* **2010**, *54*, 2517−2524.

(2) Oestereich, L.; Lüdtke, A.; Wurr, S.; Rieger, T.; Muñoz-Fontela, C.; Günther, S. Successful treatment of advanced Ebola virus infection with T-705 (favipiravir) in a small animal model. *Antiviral Res.* **2014**, *105*, 17−21.

(3) Agrawal, U.; Raju, R.; Udwadia, Z. F. Favipiravir: A new and emerging antiviral option in COVID-19. *Med. J. Armed Forces India* **2020**, *76*, 370−376.

(4) Vaidyanathan, G. Scientists criticize use of unproven COVID drugs in India. *Nature* **2020**, *587*, 187−188.

(5) Furuta, Y.; Komeno, T.; Nakamura, T. Favipiravir (T-705), a broad spectrum inhibitor of viral RNA polymerase. *Proc. Japan Acad, Ser. B* **2017**, *93*, 449−463.

(6) Yaylaci, S.; Dheir, H.; Şenocak, D.; Genc, A. B.; Kocayigit, H.; Çekiç, D.; Varım, C.; Aydın, A.; Koroglu, M.; Karabay, O. The effects of favipiravir on hematological parameters of covıd-19 patients. *Rev. Assoc. Méd. Bras.* **2020**, *66*, 65−70.

(7) Maheshwaran, S.; Akilarasan, M.; Chen, T.-W.; Chen, S.-M.; Tamilalagan, E.; Jiang, T.-Y.; Alabdullkarem, E. A.; Soylak, M. Electrocatalytic evaluation of graphene oxide warped tetragonal t-lanthanum vanadate (GO@ LaVO 4) nanocomposites for the voltammetric detection of antifungal and antiprotozoal drug (clioquinol). *Microchim. Acta* **2021**, *188*, 1−9.

(8) Qian, L.; Thiruppathi, A. R.; Elmahdy, R.; van der Zalm, J.; Chen, A. Graphene-oxide-based electrochemical sensors for the sensitive detection of pharmaceutical drug naproxen. *Sensors* **2020**, *20*, No. 1252.

(9) Chihava, R.; Apath, D.; Moyo, M.; Shumba, M.; Chitsa, V.; Tshuma, P. One-Pot Synthesized Nickel-Cobalt Sulfide-Decorated Graphene Quantum Dot Composite for Simultaneous Electrochemical Determination of Antiretroviral Drugs: Lamivudine and Tenofovir Disoproxil Fumarate. *J. Sens.* **2020**, *2020*, No. 3124102.

(10) Bharathi, G.; Lin, F.; Liu, L.; Ohulchanskyy, T. Y.; Hu, R.; Qu, J. An all-graphene quantum dot Förster resonance energy transfer (FRET) probe for ratiometric detection of HE4 ovarian cancer biomarker. *Colloids Surf., B* **2021**, *198*, No. 111458.

(11) Zhang, H.; Ba, S.; Yang, Z.; Wang, T.; Lee, J. Y.; Li, T.; Shao, F. Graphene Quantum Dot-Based Nanocomposites for Diagnosing Cancer Biomarker APE1 in Living Cells. *ACS Appl. Mater. Interfaces* **2020**, *12*, 13634−13643.

(12) Shetti, N. P.; Nayak, D. S.; Malode, S. J.; Kulkarni, R. M. Nano molar detection of acyclovir, an antiviral drug at nanoclay modified carbon paste electrode. *Sens. Bio-Sens. Res.* **2017**, *14*, 39−46.

(13) Pavamana, M.; Shetti, N. P.; Malode, S. J.; Bukkitgar, S. D. Nano level detection and analysis of an antiviral drug at ZnO nanoparticles modified sensor. *Mater. Today: Proc.* **2019**, *18*, 1568−1573.

(14) Santamaria-Fernandez, R.; Hearn, R.; Wolff, J.-C. Detection of counterfeit antiviral drug Heptodin and classification of counterfeits using isotope amount ratio measurements by multicollector inductively coupled plasma mass spectrometry (MC-ICPMS) and isotope ratio mass spectrometry (IRMS). *Sci. Justice* **2009**, *49*, 102−106.

(15) Söderström, H.; Järhult, J. D.; Olsen, B.; Lindberg, R. H.; Tanaka, H.; Fick, J. Detection of the antiviral drug oseltamivir in aquatic environments. *PLoS One* **2009**, *4*, No. e6064.

(16) Takanami, R.; Ozaki, H.; Giri, R. R.; Taniguchi, S.; Hayashi, S. Detection of antiviral drugs oseltamivir phosphate and oseltamivir carboxylate in Neya River, Osaka, Japan. *J. Water Environ. Technol.* **2010**, *8*, 363−372.

(17) Bolla, G.; Nangia, A. Pharmaceutical cocrystals: walking the talk. *Chem. Commun.* **2016**, *52*, 8342−8360.

(18) Sahoo, S. K.; Sahoo, J. K.; Panigrahi, G. K.; Pattanayak, D. K.; Rout, A. S.; Lenka, A. Preparation of graphene oxide from Bio-soot wastes: As an efficient adsorbent for highly noxious Congo red dye. *FlatChem* **2020**, *24*, No. 100198.

(19) Yang, E.; Zhang, Y.; Shen, Y. Quantum Dots for Electrochemiluminescence Bioanalysis-A Review. *Anal. Chim. Acta* **2021**, *104*, No. 339140.

(20) Wang, L.; Su, D.; Berry, S. N.; Lee, J.; Chang, Y.-T. A new approach for turn-on fluorescence sensing of l-DOPA. *Chem. Commun.* **2017**, *53*, 12465−12468.

(21) An, T.; An, J.; Gao, Y.; Li, G.; Fang, H.; Song, W. Photocatalytic degradation and mineralization mechanism and

https://doi.org/10.1021/acsanm.1c03235
ACS Appl. Nano Mater. XXXX, XXX, XXX−XXX

toxicity assessment of antivirus drug acyclovir: Experimental and theoretical studies. *Appl. Catal., B* **2015**, *164*, 279−287.
(22) Long, X.; Chen, F. Flow injection−chemiluminescence determination of acyclovir. *Luminescence* **2012**, *27*, 478−481.
(23) Skubitz, K.; Quinn, R.; Lietman, P. Rapid acyclovir radioimmunoassay, using charcoal adsorption. *Antimicrob. Agents Chemother.* **1982**, *21*, 352−354.
(24) Yeh, H. H.; Yang, Y. H.; Chen, S. H. Rapid determination of acyclovir in plasma and cerebrospinal fluid by micellar electrokinetic chromatography with direct sample injection and its clinical application. *Electrophoresis* **2006**, *27*, 819−826.
(25) Vo, H. C.; Henning, P. A.; Leung, D. T.; Sacks, S. L. Development and validation of a plasma assay for acyclovir using high-performance capillary electrophoresis with sample stacking. *J. Chromatogr. B* **2002**, *772*, 291−297.
(26) Liu, Y.; Deng, C.; Tang, L.; Qin, A.; Hu, R.; Sun, J. Z.; Tang, B. Z. Specific detection of D-glucose by a tetraphenylethene-based fluorescent sensor. *J. Am. Chem. Soc.* **2011**, *133*, 660−663.
(27) Luo, J.; Xie, Z.; Lam, J. W.; Cheng, L.; Chen, H.; Qiu, C.; Kwok, H. S.; Zhan, X.; Liu, Y.; Zhu, D.; Tang, B. Z. Aggregation-induced emission of 1-methyl-1, 2, 3, 4, 5-pentaphenylsilole. *Chem. Commun.* **2001**, 1740−1741.
(28) Chen, Y.; Lam, J. W.; Kwok, R. T.; Liu, B.; Tang, B. Z. Aggregation-induced emission: fundamental understanding and future developments. *Mater. Horiz.* **2019**, *6*, 428−433.
(29) Cai, X.; Liu, B. Aggregation-induced emission: recent advances in materials and biomedical applications. *Angew. Chem.* **2020**, *132*, 9952−9970.
(30) Kalkal, A.; Pradhan, R.; Kadian, S.; Manik, G.; Packirisamy, G. Biofunctionalized Graphene Quantum Dots Based Fluorescent Biosensor toward Efficient Detection of Small Cell Lung Cancer. *ACS Appl. Bio Mater.* **2020**, *3*, 4922−4932.
(31) Joshi, P.; Mishra, R.; Narayan, R. J. Biosensing applications of carbon-based materials. *Curr. Opin. Biomed. Eng.* **2021**, *18*, No. 100274.
(32) Hou, Y.; Lv, S.; Liu, L.; Liu, X. High-quality preparation of graphene oxide via the Hummers' method: understanding the roles of the intercalator, oxidant, and graphite particle size. *Ceram. Int.* **2020**, *46*, 2392−2402.
(33) Tetsuka, H.; Asahi, R.; Nagoya, A.; Okamoto, K.; Tajima, I.; Ohta, R.; Okamoto, A. Optically tunable amino-functionalized graphene quantum dots. *Adv. Mater.* **2012**, *24*, 5333−5338.
(34) Kim, N. H.; Kuila, T.; Lee, J. H. Simultaneous reduction, functionalization and stitching of graphene oxide with ethylenediamine for composites application. *J. Mater. Chem. A* **2013**, *1*, 1349−1358.
(35) Masteri-Farahani, M.; Askari, F. Design and photophysical insights on graphene quantum dots for use as nanosensor in differentiating methamphetamine and morphine in solution. *Spectrochim. Acta, Part A* **2019**, *206*, 448−453.
(36) Zheng, P.; Wu, N. Fluorescence and sensing applications of graphene oxide and graphene quantum dots: a review. *Chem. − Asian J.* **2017**, *12*, 2343−2353.
(37) Pavia, D. L.; Lampman, G. M.; Kriz, G. S.; Vyvyan, J. A. *Introduction to Spectroscopy*; Cengage Learning, 2014.
(38) Lee, J. U.; Lee, W.; Yi, J. W.; Yoon, S. S.; Lee, S. B.; Jung, B. M.; Kim, B. S.; Byun, J. H. Preparation of highly stacked graphene papers via site-selective functionalization of graphene oxide. *J. Mater. Chem. A* **2013**, *1*, 12893−12899.
(39) Xue, B.; Zhu, J.; Liu, N.; Li, Y. Facile functionalization of graphene oxide with ethylenediamine as a solid base catalyst for Knoevenagel condensation reaction. *Catal. Commun.* **2015**, *64*, 105−109.
(40) Gogoi, B.; Sarma, N. S. Poly-glycerol acrylate and curcumin composite: its dual emission fluorescence quenching and electrical properties for sensing 2-vinyl pyridine. *J. Mater. Sci.* **2015**, *50*, 7647−7659.
(41) Yadav, P.; Singh, A. K.; Upadhyay, C.; Singh, V. P. Photoluminescence behaviour of a stimuli responsive Schiff base: Aggregation induced emission and piezochromism. *Dyes Pigm.* **2019**, *160*, 731−739.
(42) Gogoi, B.; Sen Sarma, N. Curcumin−cysteine and curcumin−tryptophan conjugate as fluorescence turn on sensors for picric acid in aqueous media. *ACS Appl. Mater. Interfaces* **2015**, *7*, 11195−11202.
(43) Dutta, P.; Saikia, D.; Adhikary, N. C.; Sarma, N. S. Macromolecular systems with MSA-Capped CdTe and CdTe/ZnS Core/Shell quantum dots as superselective and ultrasensitive optical sensors for picric acid explosive. *ACS Appl. Mater. Interfaces* **2015**, *7*, 24778−24790.
(44) Lin, D. Q.; Brixius, P. J.; Hubbuch, J. J.; Thömmes, J.; Kula, M. R. Biomass/adsorbent electrostatic interactions in expanded bed adsorption: a zeta potential study. *Biotechnol. Bioeng.* **2003**, *83*, 149−157.
(45) Uskoković, V.; Castiglione, Z.; Cubas, P.; Zhu, L.; Li, W.; Habelitz, S. Zeta-potential and particle size analysis of human amelogenins. *J. Dent. Res.* **2010**, *89*, 149−153.
(46) Zijlstra, G.; Brandsma, C.; Harpe, M.; Van Dam, G.; Slebos, D.; Kerstjens, H.; De Boer, A.; Frijlink, H. Dry powder inhalation of hemin to induce heme oxygenase expression in the lung. *Eur. J. Pharm. Biopharm.* **2007**, *67*, 667−675.
(47) Yan, D.; Delori, A.; Lloyd, G. O.; Friščić, T.; Day, G. M.; Jones, W.; Lu, J.; Wei, M.; Evans, D. G.; Duan, X. A cocrystal strategy to tune the luminescent properties of stilbene-type organic solid-state materials. *Angew. Chem., Int. Ed.* **2011**, *50*, 12483−12486.
(48) Deka, P.; Gogoi, D.; Althubeiti, K.; Rao, D. R.; Thakuria, R. Mechanosynthesis, Characterization, and Physicochemical Property Investigation of a Favipiravir Cocrystal with Theophylline and GRAS Coformers. *Cryst. Growth Des.* **2021**, *21*, 4417−4425.
(49) Maity, D. K.; Paul, R. K.; Desiraju, G. R. Drug−Drug Binary Solids of Nitrofurantoin and Trimethoprim: Crystal Engineering and Pharmaceutical Properties. *Mol. Pharmaceutics* **2020**, *17*, 4435−4442.
(50) Chutipongtanate, S.; Thongboonkerd, V. Systematic comparisons of artificial urine formulas for in vitro cellular study. *Anal. Biochem.* **2010**, *402*, 110−112.
(51) Krebs, H. Chemical composition of blood plasma and serum. *Annu. Rev. Biochem.* **1950**, *19*, 409−430.

https://doi.org/10.1021/acsanm.1c03235
ACS Appl. Nano Mater. XXXX, XXX, XXX−XXX